ACS Photonics

Article

Cite This: ACS Photonics 2018, 5, 2402−2407

Ultra-High-Efficiency Anomalous Refraction with Dielectric Metasurfaces

David Sell,[†,§] Jianji Yang,[‡,§] Evan W. Wang,[‡,§] Thaibao Phan,[‡] Sage Doshay,[†] and Jonathan A. Fan*[,‡]

[†]Department of Applied Physics, Stanford University, Stanford, California 94305, United States

[‡]Department of Electrical Engineering, Stanford University, Stanford, California 94305, United States

Supporting Information

ABSTRACT: Anomalous refraction is a form of extreme waveform manipulation that can be realized with artificially structured nanomaterials, such as metamaterials or metasurfaces. While this phenomenon has been previously demonstrated for select input and output angles, its generalization to arbitrary angles with high efficiencies remains a challenge. In this study, we show that periodic dielectric metasurfaces can support ultra-high-efficiency anomalous refraction for nearly arbitrary combinations of incident and outgoing angles (>90% efficiency for angles up to 50°). Both polarization-dependent and polarization-independent device configurations can be realized, and the achieved metrics exceed the capabilities of conventional metasurfaces by a large margin. Many of the devices studied here utilize dielectric nanostructures that support strong near-field optical interactions with neighboring structures and complex optical mode dynamics. We envision that these concepts can be integrated with practical applications in optical communications, spectroscopy, and laser optics.

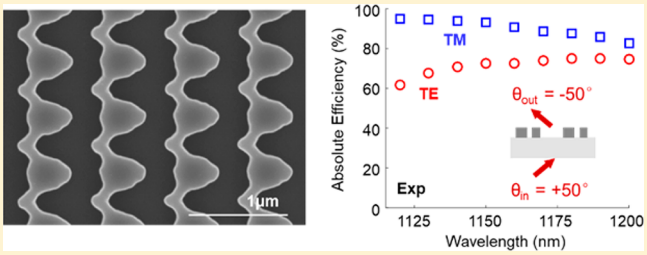

KEYWORDS: *metasurface, metagrating, anomalous refraction, diffraction, high efficiency, dielectric antenna, optimization*

Devices that exhibit anomalous refraction, in which the angles of an incident and transmitted electromagnetic wave have opposite signs, are an important subset of wavefront engineering devices. Scientifically, devices supporting anomalous refraction have served as model systems to study the extent to which nanocomposite materials can manipulate wavefronts in extreme ways. Technologically, these types of devices serve as important components in optical communications,[1] laser optics,[2] and pulse compression[3] systems. In all of these applications, high efficiency is a strict requirement.

One approach to realizing anomalous refraction is with nanostructured bulk media. Metamaterials supporting negative permittivity and permeability at a target wavelength have a negative index of refraction and can steer light to negative angles.[4,5] Anisotropic hyperbolic metamaterials with a negative permittivity along one or two geometric axes support hyperbolic isofrequency contours, which can enable negative refraction for select device orientations and incident angles.[6,7] Photonic crystals consisting solely of dielectrics can also be configured to support negative refraction.[8,9] While these systems have served as successful proof-of-concept realizations of anomalous refraction, impedance matching issues and absorption losses have limited their efficiencies.

A complementary approach is to utilize thin-film diffractive elements. Early realizations of such devices include the implementation of conventional transmissive or reflective diffractive gratings in the Littrow configuration.[10,11] Here, high-efficiency beam steering at modest angles can be obtained, but the incident and outgoing angles are restricted to be equal and opposite. More recently, optical metasurfaces have been developed as a versatile platform for wavefront engineering and can produce devices supporting generalized laws of refraction, including anomalous refraction.[12−16] This design platform has since been extended to a broad range of optical technologies including metalenses,[17−20] holograms,[21−24] polarizers,[25,26] beam splitters,[27−29] and beam deflectors.[30−35]

Initial conceptions of metasurfaces utilize a set of subwavelength-scale elements, such as nanowaveguides or nanoresonators, each designed to impart a discrete phase response to the incident field. When stitched together into ensembles, these elements cumulatively serve as nanoscale phased arrays. While this design approach is effective for many wavefront engineering problems, limitations exist for extreme beam manipulation, when the differences between the input and output angles are large.[34,36] For example, the deflection efficiencies of periodic metasurfaces (i.e., metagratings) based on this phased array method are poor for very wide deflection angles,[27,31,33] due to undesired light coupling into spurious diffraction orders. Recent theoretical work suggests that these limitations originate because this design method does not properly manage the impedance mismatch between the incident and desired wave fronts, particularly in the limit of extreme beam manipulation.[36,37] As such, dielectric metasurfaces based on the phased array method have yet to produce

Received: February 8, 2018
Published: March 15, 2018

DOI: 10.1021/acsphotonics.8b00183
ACS Photonics 2018, 5, 2402−2407

demonstrations of high-efficiency anomalous refraction, and it remains unclear if or how this phenomenon can be realized.

In this study, we theoretically and experimentally show that dielectric metagratings can yield ultra-high-efficiency anomalous refraction for nearly arbitrary input and output angles. These devices operate by deflecting a plane wave, incident at a positive angle, to the −1 diffraction order (Figure 1). High

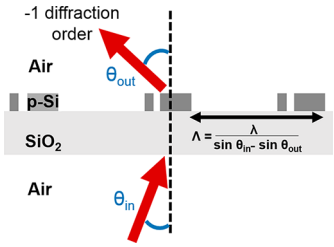

Figure 1. Anomalous refraction is achieved with a metagrating by deflecting an incident plane wave to the −1 diffraction order. The period of the metagrating, Λ, is set by the incident angle θ_{in}, outgoing angle θ_{out}, and free space wavelength λ.

efficiencies are made possible by nontrivial optical mode dynamics supported within these devices, which are fine-tuned through careful specification of their optical mode profiles. As a demonstration, we examine metagratings comprising polycrystalline silicon (poly-Si) ridges that can deflect polarized near-infrared light to negative angles. We also show that high-efficiency devices supporting polarization-independent anomalous refraction can be realized.

We begin by theoretically examining metagratings consisting of poly-Si nanoridges that deflect plane waves (λ_0 = 840 nm, TM polarization) to negative angles. To provide a detailed analysis on a representative model system, we focus on devices that deflect radiation from an incident angle θ_{in} = +20° to an outgoing angle θ_{out} = −40°. Devices based on high-aspect-ratio silicon nanowaveguides as phased array elements are not capable of high-efficiency beam deflection for these angles (Figure S1). While the specific geometries and optical modes in this analysis are particular to these angles, the observed requirement of nonintuitive nanoridge layouts and complex optical dynamics for high-efficiency anomalous refraction is general and applies to devices supporting other θ_{in}'s and θ_{out}'s. For these angles, the period is relatively short ($\Lambda \approx 1.02\lambda_0 \approx$ 860 nm), and such devices based on the traditional phased-array approach support two ridges per period. Thus, for our starting model system, we adopt a two-ridge design and seek to optimize its performance.

To search for device configurations with high efficiencies, we perform a parametric sweep of the ridge thickness, widths w_1 and w_2 of the two ridges, and S, which is the smaller of the two distances separating the ridges. The absolute deflection efficiencies of optimal devices as a function of S are plotted in Figure 2a. Absolute efficiency is defined as the energy transmitted to the desired angle divided by the energy of the incident wave in the substrate. A ridge thickness of 325 nm is chosen because it produces devices with the highest performance for the given wavelength and function (Figure S2). In the regime of wide separation (i.e., $S \approx$ 300 nm), the deflection efficiencies are relatively low and are well below 50%. However, as S approaches 90 nm, the absolute efficiencies increase and reach maximum values near 96%. The quality of beam deflection supported by the optimal device with S = 90 nm can be visualized in an electromagnetic field plot (Figure 2b), which displays well-defined wavefronts propagating in the incident and outgoing directions.

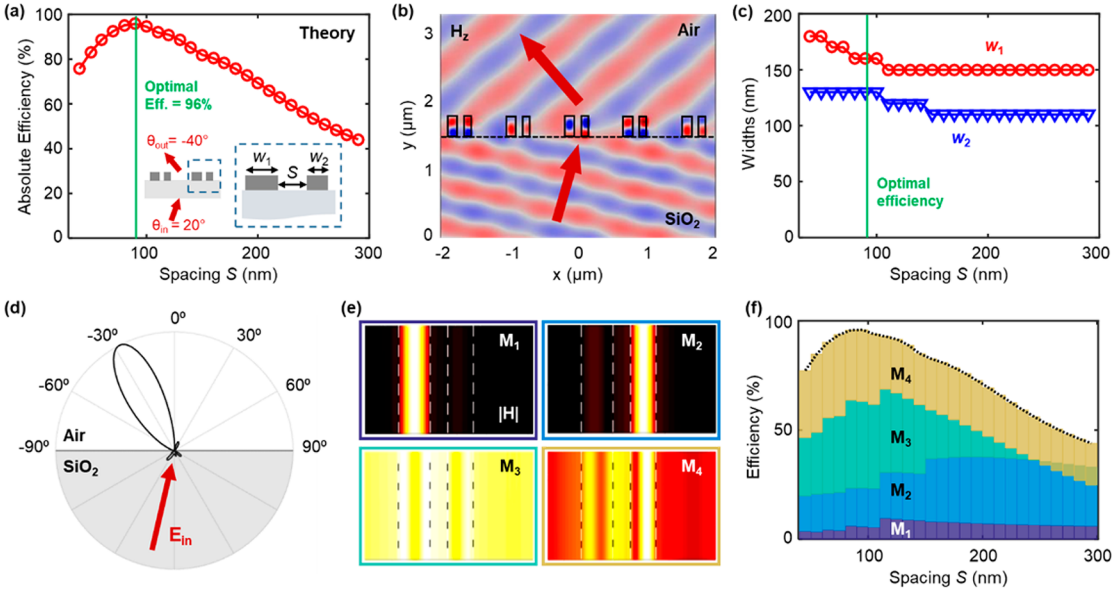

Figure 2. Theoretical analysis of metagratings supporting θ_{in} = +20° and θ_{out} = −40°. (a) Calculated absolute efficiencies of a metagrating, comprising two nanoridges per period with optimized ridge widths, as a function of nanoridge spacing S. The incident waves are TM-polarized. The globally optimized metagrating exhibits absolute efficiencies near 96% (green line). Inset: Schematic of an individual grating period. (b) Field plot of a plane wave incident on a globally optimized metagrating. (c) Ridge widths w_1 and w_2 that yield devices with optimal absolute efficiencies, plotted in (a), for a given S. (d) Far-field profile based on a full-wave simulation of a plane wave incident on an isolated set of optimized coupled nanoridges (green line in (c)), showing strong light deflection to negative outgoing angles. (e) Top views of the field profiles of the propagating supermodes, solved for the globally optimized metagrating. The plots each span an individual grating period, and the dashed lines demarcate the boundaries of the silicon ridges. (f) Contribution of individual modes to deflection efficiency for devices with optimized ridge widths and differing S.

DOI: 10.1021/acsphotonics.8b00183
ACS Photonics 2018, 5, 2402−2407

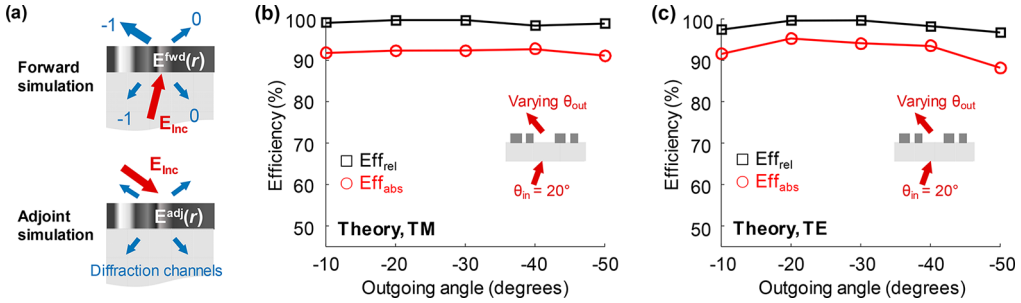

Figure 3. Silicon nanoridge-based devices supporting generalized anomalous refraction. (a) Schematics of the forward and adjoint simulations used in the topology optimization of metagratings. (b, c) Absolute and relative efficiencies of sets of metagratings designed using topology optimization for (b) TM-incident waves with λ = 840 nm and (c) TE-incident waves with λ = 1440 nm. In both plots, θ_{in} = +20° and θ_{out} is varied between −10° and −50°.

The combinations of w_1 and w_2 that yield the optimal deflection efficiencies in Figure 2a are presented in Figure 2c. Interestingly, the dimensions of the ridge widths are consistently similar, and they are unchanged across large ranges of S values. An analysis of deflectors with fixed ridge widths and decreasing S (Figure S3) also displays efficiency trends following those in Figure 2a. These plots indicate that while slight adjustments to the ridge widths are necessary to refine device performance, high deflection efficiencies in this system are principally enabled by optical dynamics sensitive to near-field coupling between the ridges.

The observed high deflection efficiencies can be traced to the optical response of isolated coupled ridges, which serve as nanoscale antennas. To probe this further, we perform full-wave simulations of a plane wave incident on an individual optimized antenna with S = 90 nm. The far-field profile of the combined incident, transmitted, and scattered fields, calculated using a near-to-far-field transformation,[38] is plotted in Figure 2d and displays a number of interesting features. First, it exhibits a large lobe at negative angles, indicating that individual antennas can efficiently deflect radiation to negative angles. Second, it shows minimal reflection of the incident plane wave at the substrate−air interface, indicating strong impedance matching by our antenna at the air−substrate interface. Third, there is strongly suppressed plane wave transmission to positive angles, indicating that the antenna supports a scattering profile that destructively interferes with the transmitted incident field.

To further elucidate the origins of high-efficiency anomalous refraction, we solve for and visualize the supermodes of antennas with S = 90 nm arranged in a periodic wavelength-scale lattice. Since neighboring antennas in this configuration are widely spaced and experience minimal near-field coupling, this antenna array study highlights the underlying physical operation of individual antennas. We set the period to be the same as in Figure 2b, though our findings generally apply to a wide range of periods (see Figure S4). The modes of this antenna array are plotted in Figure 2e. Modes M_1 and M_2 have fields that are located principally in the individual ridges and are not strongly impacted by their close proximity. Modes M_3 and M_4, on the other hand, have fields that are spatially distributed across the antenna and that support strong near-field coupling between the ridges.

To understand the impact of each mode in the beam deflection process, we calculate the contribution of individual modes to the overall deflection efficiency for the optimal S = 90 nm device and also for the range of devices simulated in Figure 2c. For each device geometry, we first assume that the incident electromagnetic plane wave couples to only M_1, and we calculate the resulting fraction of incident power that deflects to the desired angle. This value represents the efficiency contributed by M_1. We then include more modes in order of increasing mode number, M_i, and record the net change in device efficiency with the addition of each mode. The results are summarized in Figure 2f and indicate that all the modes work collectively to realize anomalous refraction. Modes M_3 and M_4 in particular strongly contribute to beam deflection efficiency in the globally optimal device configurations, in a manner that is highly sensitive to S. As such, high-efficiency beam deflection requires the fine-tuning of near-field optical coupling between ridges, which is critical to specifying M_3 and M_4 and their detailed interactions with M_1 and M_2. A more rigorous quantification of these detailed optical dynamics is in the Supporting Information.

Our observation of directional beam deflection based on interference between differing optical modes appears related to other established schemes, such as those utilizing interfering electric and magnetic dipole modes.[39] While there are qualitative similarities, our system utilizes a larger number of modes, as well as strong intramode and intermode coupling.[33]

In this model system, only two coupled nanoridges per period are required to produce high-efficiency anomalous refraction. For other incident or outgoing angles, different numbers of ridges, ridge widths, and spacings may be required. For example, devices that steer light to smaller angles contain larger periods and typically require more ridges to efficiently deflect the incident field. While a parametric sweep can be performed for each desired optical function to identify suitable geometric configurations of coupled ridges, the problem quickly becomes intractable as the number of parameters increases. We therefore turn to topology optimization, which is an iterative, computationally efficient mathematical method that can produce high-performance metasurfaces without prior assumptions of their topology or operating mechanisms.[27,28,33,40,41] This design method also permits the incorporation of fabrication constraints, to ensure that the designs are robust to nanofabrication errors.[42] To summarize its use here, we iteratively evolve a device consisting of a dielectric continuum with values between ε_{Si} and ε_{air} to one consisting of only ε_{Si} and ε_{air}. Two simulations are performed each iteration, a forward simulation of a plane wave incident from the substrate based on our desired input angle and an adjoint simulation of a plane wave incident from air at our desired outgoing angle (Figure 3a). The electric fields in the device layer are recorded for each simulation, and they are used to calculate perturbative

DOI: 10.1021/acsphotonics.8b00183
ACS Photonics 2018, 5, 2402−2407

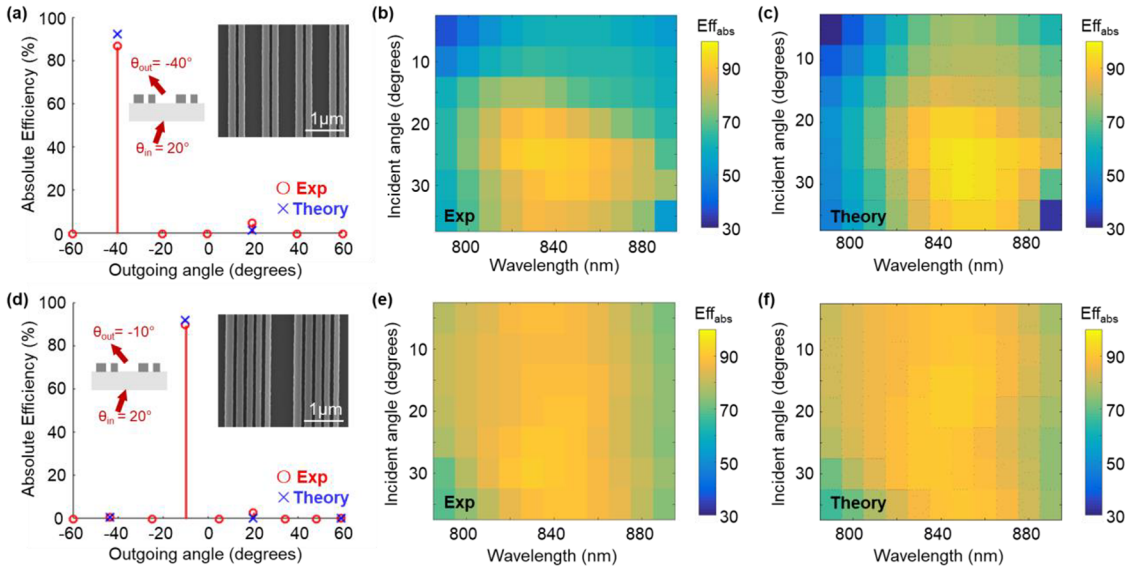

Figure 4. Experimental analysis of nanoridge-based metagratings. (a) Experimentally measured absolute efficiency as a function of output angle, for a device that deflects an incident TM-polarized plane wave (λ = 840 nm) with θ_{in} = +20° to θ_{out} = −40°. The device has the same geometric parameters as the globally optimized device featured in Figure 2. The absolute efficiency is near 90%. Inset: SEM image of a top view of the device. (b, c) Absolute deflection efficiencies for a range of incident angles and wavelengths, which are (b) experimentally measured from the device in (a), and (c) theoretically calculated. (d−f) Experimental analysis similar to (a)−(c) for a device that deflects an incident TM-polarized plane wave (λ = 840 nm) with θ_{in} = +20° to θ_{out} = −10°.

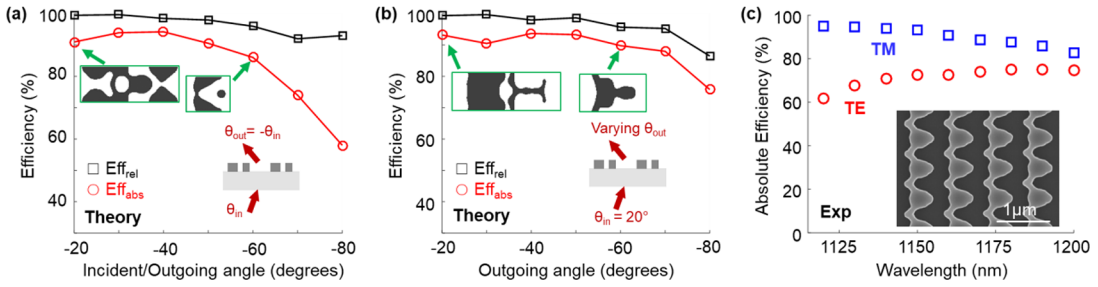

Figure 5. Topology-optimized silicon devices supporting generalized, polarization-independent anomalous refraction. (a, b) Absolute and relative efficiencies of metagratings designed for (a) θ_{in} and θ_{out} that have equal magnitude but opposite sign and (b) θ_{in} = +20° and θ_{out} ranging from −20° to −80°. The efficiencies in the plots represent averages for TE- and TM-polarized incident waves. Insets: Top view images of individual metagrating unit cells. (c) Experimental absolute efficiencies of a device designed for θ_{in} = +50° and θ_{out} = −50°, for differing incident polarizations and wavelengths. Inset: SEM image of a top view of the device.

modifications to the dielectric constant at each point in the device, which combine to increase device efficiency as the simulation progresses.

The theoretical performances of nanoridge-based devices that deflect TM-polarized plane waves with θ_{in} = +20° and λ_0 = 840 nm to differing outgoing angles, designed using topology optimization, are summarized in Figure 3b. For this plot, we include both the absolute efficiency as well as the relative efficiency, which is the energy transmitted to the desired angle divided by the total transmitted energy. The absolute efficiency of all the devices is over 90%, and the relative efficiencies are near unity, indicating that ultra-high-efficiency anomalous refraction devices for more general input and output angles can be realized with coupled dielectric ridges. This design methodology also extends to devices that support high-efficiency anomalous refraction for TE-polarized plane waves (Figure 3c), indicating the versatility and broad applicability of topology optimization to these classes of devices. The number of ridges for these devices range from two to five (see Table S1 for geometric parameters). In all cases, strong near-field optical coupling between ridges is observed and the optical dynamics are complex (see Figure S5 for a rigorous analysis of TM-polarized θ_{out} = −10° device), which is consistent with our model system from earlier.

To experimentally verify the viability of our designs, we fabricate and characterize metagratings supporting anomalous refraction. A more thorough discussion of the experimental details can be found in ref 27. To summarize, we first grow a layer of poly-Si via chemical vapor deposition on a silicon dioxide substrate. The metagrating designs are then patterned using electron beam lithography and reactive ion etching. To characterize these devices, we loosely focus a tunable white-light laser beam on the devices, and we detect the diffracted beams using a germanium photodetector mounted on a goniometer. Power measurements of the incident beam transmitted through air, together with calculated reflectivity values at the air−substrate interface for the given incidence angle, are used to calibrate our efficiency values.

Far-field profiles of two devices designed for θ_{in} = +20°, one that deflects TM-polarized waves to θ_{out} = −40° and the other

DOI: 10.1021/acsphotonics.8b00183
ACS Photonics 2018, 5, 2402−2407

to $\theta_{out} = -10°$, are plotted in Figure 4a and d, respectively. The experimental efficiencies for each device are near or above 90% and are well within 10% of the theoretical value, indicating that ultra-high-efficiency devices can be experimentally realized with proper fabrication processing. Additional measurements are performed by sweeping the wavelengths and incident angles around their target parameters, and the resulting efficiency maps are plotted in Figure 4b and e. These plots demonstrate good agreement with theoretical values (Figure 4c and f). The low-angle deflector (Figure 4e) supports high efficiencies over a large angular bandwidth, in part because for small θ_{out} the orientation of the wavevector of the outgoing plane wave changes a relatively small amount as θ_{in} varies.

High-efficiency polarization-independent devices supporting anomalous refraction can be realized by applying topology optimization to fully three-dimensional layouts. These devices are designed to be 325 nm thick, with a minimum feature size constraint of 60 nm enforced during the simulation process, to match our fabrication limitations. The resulting devices comprise highly complex curvilinear shapes and, in many cases, utilize strong near-field coupling between neighboring dielectric structures. Compared to the devices based on ridges presented earlier, which are designed to operate for a specific polarization, the additional degrees of freedom in fully three-dimensional layouts enable polarization-independent operation. The theoretical performances of devices that deflect unpolarized plane waves with $\lambda_0 = 1150$ nm to a wide range of θ_{in} and θ_{out} are summarized in Figure 5a and b. These devices exhibit efficient polarization-independent deflection with efficiencies near or above 90% for angles less than 60°. For $\theta_{inc} = +60°$ and $\theta_{out} = -60°$, the device demonstrates a polarization-independent absolute efficiency of 86%, compared to the single-polarization deflection efficiency of 85% presented in ref 10. Even for deflection configurations as extreme as $\theta_{inc} = +80°$ and $\theta_{out} = -80°$, absolute efficiencies above 50% can be obtained.

A representative topology-optimized device made from poly-Si, with $\theta_{inc} = +50°$ and $\theta_{out} = -50°$, is shown in Figure 5c and displays a curvilinear spatial profile. Plots of experimental absolute efficiencies for each polarization as a function of incident wavelength display high overall efficiencies. For TM-incident polarized waves, the experimental efficiencies from 1100 to 1180 nm are exceptionally high and are well above 90%. The efficiencies for TE-polarized incident waves are lower, which is due in part to the relatively high sensitivity of TE modes to fabrication imperfections, arising from the strong localization of these modes in silicon. Additional experimental measurements of this device are in Figure S7.

In summary, we have shown that metagratings can be designed to support generalized anomalous refraction capabilities with ultrahigh efficiencies. Topology optimization serves as an effective and computationally efficient design method to produce these device designs for both polarized and unpolarized input waves. This work more generally shows that the performance of dielectric metasurfaces at optical frequencies can be dramatically enhanced through the utilization of light−matter interactions that go beyond those featured in conventional phased array designs. By utilizing nontrivial optical mode dynamics, which are fine-tuned through careful specification of their optical mode profiles, new regimes of device designs can be accessed that push the limits of extreme wavefront control.

■ ASSOCIATED CONTENT

Supporting Information

The Supporting Information is available free of charge on the ACS Publications website at DOI: 10.1021/acsphotonics.8b00183.

Benchmark of devices based on conventional metasurfaces; additional analysis of high-efficiency ridge-based metasurfaces; geometric parameters of topology-optimized devices; additional experimental data of three-dimensional metasurfaces; Figures S1−S7 (PDF)

■ AUTHOR INFORMATION

Corresponding Author

*E-mail: jonfan@stanford.edu.

ORCID

Jianji Yang: 0000-0003-3903-5094

Jonathan A. Fan: 0000-0001-9816-9979

Author Contributions

§D. Sell, J. Yang, and E. W. Wang contributed equally to this work.

Notes

The authors declare no competing financial interest.

■ ACKNOWLEDGMENTS

This work was supported by the Office of Naval Research (N00014-16-1-2630) and the Packard Fellowship Foundation. The samples in this study were fabricated at the Stanford Nanofabrication Facility and Stanford Nano Shared Facility. The simulations were performed in the Sherlock computing cluster at Stanford University. D.S. acknowledges support by the National Science Foundation (NSF) through the NSF Graduate Research Fellowship, and S.D. acknowledges support by the Department of Defense through the National Defense Science and Engineering Graduate Fellowship Program. We acknowledge J. Jiang for simulations of anomalous refraction devices based on conventional phased arrays and R. Yang for polycrystalline silicon growth.

■ REFERENCES

(1) Rose, B.; Rasmussen, T.; Khalfaoui, C.; et al. US Patent 6978062B2, 2005.

(2) Hawthorn, C. J.; Weber, K. P.; Scholten, R. E. Littrow configuration tunable external cavity diode laser with fixed direction output beam. *Rev. Sci. Instrum.* **2001**, *72*, 4477−4479.

(3) Rhee, J.-K.; Sosnowski, T. S.; Norris, T. B.; et al. Chirped-pulse amplification of 85-fs pulses at 250 kHz with third-order dispersion compensation by use of holographic transmission gratings. *Opt. Lett.* **1994**, *19*, 1550−1552.

(4) Smith, D. R.; Pendry, J. B.; Wiltshire, M. C. K. Metamaterials and Negative Refractive Index. *Science* **2004**, *305*, 788−792.

(5) Valentine, J.; Zhang, S.; Zentgraf, T.; et al. Three-dimensional optical metamaterial with a negative refractive index. *Nature* **2008**, *455*, 376.

(6) Hoffman, A. J.; Alekseyev, L.; Howard, S. S.; et al. Negative refraction in semiconductor metamaterials. *Nat. Mater.* **2007**, *6*, 946.

(7) Yao, J.; Liu, Z.; Liu, Y.; et al. Optical Negative Refraction in Bulk Metamaterials of Nanowires. *Science* **2008**, *321*, 930−930.

(8) Luo, C.; Johnson, S. G.; Joannopoulos, J. D.; et al. All-angle negative refraction without negative effective index. *Phys. Rev. B: Condens. Matter Mater. Phys.* **2002**, *65*, 201104.

(9) Cubukcu, E.; Aydin, K.; Ozbay, E.; et al. Negative refraction by photonic crystals. *Nature* **2003**, *423*, 604.

DOI: 10.1021/acsphotonics.8b00183
ACS Photonics 2018, 5, 2402−2407

(10) Clausnitzer, T.; Kampfe, T.; Kley, E. B.; et al. Investigation of the polarization-dependent diffraction of deep dielectric rectangular transmission gratings illuminated in Littrow mounting. *Appl. Opt.* **2007**, *46*, 819−826.
(11) Hehl, K.; Bischoff, J.; Mohaupt, U.; et al. High-efficiency dielectric reflection gratings: design, fabrication, and analysis. *Appl. Opt.* **1999**, *38*, 6257−6271.
(12) Yu, N.; Genevet, P.; Kats, M. A.; et al. Light Propagation with Phase Discontinuities: Generalized Laws of Reflection and Refraction. *Science* **2011**, *334*, 333−337.
(13) Genevet, P.; Capasso, F.; Aieta, F.; et al. Recent advances in planar optics: from plasmonic to dielectric metasurfaces. *Optica* **2017**, *4*, 139−152.
(14) Sun, S.; Yang, K.-Y.; Wang, C.-M.; et al. High-Efficiency Broadband Anomalous Reflection by Gradient Meta-Surfaces. *Nano Lett.* **2012**, *12*, 6223−6229.
(15) Nemilentsau, A.; Low, T. Broadband Achromatic Anomalous Mirror in Near-IR and Visible Frequency Ranges. *ACS Photonics* **2017**, *4*, 1646−1652.
(16) Grady, N. K.; Heyes, J. E.; Chowdhury, D. R.; et al. Terahertz Metamaterials for Linear Polarization Conversion and Anomalous Refraction. *Science* **2013**, *340*, 1304−1307.
(17) Khorasaninejad, M.; Chen, W. T.; Devlin, R. C.; et al. Metalenses at visible wavelengths: Diffraction-limited focusing and subwavelength resolution imaging. *Science* **2016**, *352*, 1190−1194.
(18) Lin, D.; Fan, P.; Hasman, E.; et al. Dielectric gradient metasurface optical elements. *Science* **2014**, *345*, 298−302.
(19) Zhan, A.; Colburn, S.; Trivedi, R.; et al. Low-Contrast Dielectric Metasurface Optics. *ACS Photonics* **2016**, *3*, 209−214.
(20) Arbabi, E.; Arbabi, A.; Kamali, S. M.; et al. Multiwavelength polarization-insensitive lenses based on dielectric metasurfaces with meta-molecules. *Optica* **2016**, *3*, 628−633.
(21) Wang, L.; Kruk, S.; Tang, H.; et al. Grayscale transparent metasurface holograms. *Optica* **2016**, *3*, 1504−1505.
(22) Khorasaninejad, M.; Ambrosio, A.; Kanhaiya, P. et al.. Broadband and chiral binary dielectric meta-holograms. *Sci. Adv.* **2016**, *2*, e150125810.1126/sciadv.1501258.
(23) Wen, D.; Yue, F.; Li, G.; et al. Helicity multiplexed broadband metasurface holograms. *Nat. Commun.* **2015**, *6*, 8241.
(24) Kim, J.; Li, Y.; Miskiewicz, M. N.; et al. Fabrication of ideal geometric-phase holograms with arbitrary wavefronts. *Optica* **2015**, *2*, 958−964.
(25) Yang, Y.; Wang, W.; Moitra, P.; et al. Dielectric Meta-Reflectarray for Broadband Linear Polarization Conversion and Optical Vortex Generation. *Nano Lett.* **2014**, *14*, 1394−1399.
(26) Shen, B.; Wang, P.; Polson, R.; et al. Ultra-high-efficiency metamaterial polarizer. *Optica* **2014**, *1*, 356−360.
(27) Sell, D.; Yang, J.; Doshay, S.; et al. Large-Angle, Multifunctional Metagratings Based on Freeform Multimode Geometries. *Nano Lett.* **2017**, *17*, 3752−3757.
(28) Sell, D.; Yang, J.; Doshay, S.; et al. Periodic Dielectric Metasurfaces with High-Efficiency, Multiwavelength Functionalities. *Adv. Opt. Mater.* **2017**, *5*, 1700645.
(29) Khorasaninejad, M.; Zhu, W.; Crozier, K. B. Efficient polarization beam splitter pixels based on a dielectric metasurface. *Optica* **2015**, *2*, 376−382.
(30) Sell, D.; Yang, J.; Doshay, S.; et al. Visible Light Metasurfaces Based on Single-Crystal Silicon. *ACS Photonics* **2016**, *3*, 1919−1925.
(31) Yang, J.; Fan, J. A. Topology-optimized metasurfaces: impact of initial geometric layout. *Opt. Lett.* **2017**, *42*, 3161−3164.
(32) Yang, J.; Fan, J. A. Analysis of material selection on dielectric metasurface performance. *Opt. Express* **2017**, *25*, 23899−23909.
(33) Yang, J.; Sell, D.; Fan, J. A. Freeform Metagratings Based on Complex Light Scattering Dynamics for Extreme, High Efficiency Beam Steering. *Ann. Phys.* **2018**, *530*, 1700302.
(34) Ra'di, Y.; Sounas, D. L.; Alù, A. Metagratings: Beyond the Limits of Graded Metasurfaces for Wave Front Control. *Phys. Rev. Lett.* **2017**, *119*, 067404.
(35) Zhu, L.; Kapraun, J.; Ferrara, J.; et al. Flexible photonic metastructures for tunable coloration. *Optica* **2015**, *2*, 255−258.
(36) Asadchy, V. S.; Albooyeh, M.; Tcvetkova, S. N.; et al. Perfect control of reflection and refraction using spatially dispersive metasurfaces. *Phys. Rev. B: Condens. Matter Mater. Phys.* **2016**, *94*, 075142.
(37) Asadchy, V. S.; Wickberg, A.; Díaz-Rubio, A.; et al. Eliminating Scattering Loss in Anomalously Reflecting Optical Metasurfaces. *ACS Photonics* **2017**, *4*, 1264−1270.
(38) Yang, J.; Hugonin, J.-P.; Lalanne, P. Near-to-Far Field Transformations for Radiative and Guided Waves. *ACS Photonics* **2016**, *3*, 395−402.
(39) Staude, I.; Miroshnichenko, A. E.; Decker, M.; et al. Tailoring Directional Scattering through Magnetic and Electric Resonances in Subwavelength Silicon Nanodisks. *ACS Nano* **2013**, *7*, 7824−7832.
(40) Jensen, J. S.; Sigmund, O. Topology optimization for nano-photonics. *Laser & Photonics Reviews* **2011**, *5*, 308−321.
(41) Piggott, A. Y.; Lu, J.; Lagoudakis, K. G.; et al. Inverse design and demonstration of a compact and broadband on-chip wavelength demultiplexer. *Nat. Photonics* **2015**, *9*, 374.
(42) Schevenels, M.; Lazarov, B. S.; Sigmund, O. Robust topology optimization accounting for spatially varying manufacturing errors. *Computer Methods in Applied Mechanics and Engineering* **2011**, *200*, 3613−3627.

DOI: 10.1021/acsphotonics.8b00183
ACS Photonics 2018, 5, 2402−2407